JOURNAL OF PROPULSION AND POWER
Vol. 26, No. 4, July–August 2010

Microstructure Effects in Aluminized Solid Rocket Propellants

L. T. DeLuca,* L. Galfetti,† G. Colombo,‡ F. Maggi,§ and A. Bandera¶
Politecnico di Milano, I-20156 Milan, Italy
V. A. Babuk**
Baltic State Technical University, 190005, Saint Petersburg, Russia
and
V. P. Sinditskii††
Mendeleev University of Chemical Technology, 125047, Moscow, Russia

DOI: 10.2514/1.45262

Experiments concerning the ballistic characterization of several nanoaluminum (*n*Al) powders are reported. Most studies were performed with laboratory composite solid rocket propellants based on ammonium perchlorate as oxidizer and hydroxyl-terminated polybutadiene as inert binder. The ultimate objective is to understand the flame structure of differently metallized formulations and improve their specific impulse efficiency by mitigating the two-phase losses. Ballistic results confirm, for increasing *n*Al mass fraction or decreasing *n*Al size, higher steady burning rates with essentially the same pressure sensitivity and reduced average size of condensed combustion products. However, aggregation and agglomeration phenomena near the burning surface appear noticeably different for microaluminum (μAl) and *n*Al powders. By contrasting the associated flame structures, a particle-laden flame zone with a sensibly reduced particle size is disclosed in the case of *n*Al. Propellant microstructure is considered the main controlling factor. A way to predict the incipient agglomerate size for μAl propellants is proposed and verified by testing several additional ammonium perchlorate/hydroxyl-terminated polybutadiene/aluminum formulations of industrial manufacture.

Nomenclature

a	=	multiplier factor Vieille law, $(\text{mm/s})/(\text{bar})^n$
D	=	particle diameter, μm
n	=	steady burning rate pressure sensitivity
nAl	=	nanosized aluminum
p	=	pressure, bar
r_b	=	propellant steady burning rate, mm/s
μAl	=	microsized aluminum

I. Introduction

WHILE metal mirrors of 0.01 μm thickness have been known for centuries, the first investigation on submicron Al powder for energetic applications was carried out in Russia by Gen et al. [1] in 1978. They used *n*Al produced by vaporization and consequent condensation of the metal vapors in argon, a method already developed [2] by Gen et al. in 1959. A remarkable decrease of dimensions of the Al burning condensed products was observed. The idea of applying nanosized particulate metals as ingredients to radically improve performance of high-energy materials was introduced in the 1980s, mainly by Ivanov and Tepper [3] in Russia and Barbee [4] in the United States. Ivanov preeminently used for production the electrical wire explosion (EEW) process, whereas Barbee worked with multilayer packs of nanoscale metal mirrors for an initiator device.

Later research activities pointed out that nanosized particles can be divided into coarse and fine particles, with a border size of about 10 nm. While for particles larger than 10 nm distinctive features are mainly determined by their specific surface, for the second group (made by particles containing tens of subparticles) an increase of energy takes place due to intermolecular interactions. In particular, for Al particles of the second group the enthalpy of formation can reach [5] values of the order of MJ/kg. The current high interest in nanoparticles in general is motivated from both applied and fundamental reasons [6].

The aim of this research program is to experimentally assess the influence of Al particle size on the ballistic properties and flame structure of solid rocket propellants. While the physical characterization of *n*Al powders and analyses of solid combustion residues were discussed previously [7–10], the companion ample agglomeration study conducted for a variety of industrial μAl propellants is only briefly discussed in this paper.

In this paper the measured steady ballistic properties of many laboratory μAl and *n*Al formulations are presented. After detailing the tested solid propellant formulations, the distinctly different ballistic properties observed for μAl vs *n*Al formulations are discussed. The achieved results, while in agreement with literature trends, are explained in terms of the propellant microstructure (that is the fine material distributed among the coarse oxidizer particles). In this respect, strikingly different features are exhibited by the tested μAl vs *n*Al formulations when examined by high-speed and high-resolution video camera recordings. Mastering of theses effects opens the way to innovative fine tuning of solid rocket motor performance. Concluding remarks and hints of future work complete the paper.

II. Solid Rocket Propellant Features

Combustion of metallized solid rocket propellants leads to the formation of condensed combustion products, which have a critical influence on rocket motor performance. Condensed combustion

Received 3 May 2009; revision received 28 January 2010; accepted for publication 8 March 2010.

*Professor, Space Propulsion and Nanoenergetics Laboratory, 34 Via La Masa. Associate Fellow AIAA.
†Professor, Space Propulsion and Nanoenergetics Laboratory, 34 Via La Masa.
‡Senior Technician, Space Propulsion and Nanoenergetics Laboratory, 34 Via La Masa.
§Research Fellow, Space Propulsion and Nanoenergetics Laboratory, 34 Via La Masa, Member AIAA.
¶Ph.D. Candidate, Space Propulsion and Nanoenergetics Laboratory, 34 Via La Masa.
**Professor, Aerospace Division, Department of Space Vehicles and Rocket Motors, 1 First Krasnoarmeyskaya Street.
††Professor, Department of Chemical Engineering, 9 Miusskaya Square.

Table 1 Summary of Al powders currently under investigation and nomenclature

Space Propulsion and Nanoenergetics Laboratory Log	*Country (source)* Production technique[a]; coating; nominal diameter[b]	BET surface m^2/g	BET diameter μm
Type 01	*Russia (SibTermoChim) similar to Alex®*	——	——
Al_01a	EEW; uncoated; nominal size: 0.15 μm	15.3 ± 0.15	0.145
Type 02	*Russia (Institute of High Current Electronics, RAS)*	——	——
Al_02b	EEW; uncoated; nominal size: 0.15 μm; production: 2002	14.4 ± 0.07	0.154
Type 03	*Russia (Tomsk State University)*	——	——
Al_03d	Pneumatic mill; uncoated; nominal size: 2.5 μm	0.73 ± 0.01	3.035
Type 04	*Russia (Peter's Research Center)*	——	——
Al_04a	Plasma condensation; coated; nominal size: 0.20 μm	6.10 ± 0.06	0.363
Type 05	*UK (space industry supplier)*	——	——
Al_05a	spherical; uncoated; nominal size: 30 μm	$\approx 0.10 \pm 0.01$	22.157
Type 06	*Italy (commercial supplier)*	——	——
Al_06	flakes; uncoated; nominal size: 50 μm	<0.10[c]	NAv
Type 09	*USA (AMCOM)*	——	——
Al_09a	Plasma condensation; uncoated; nominal size: 0.09 μm	23.6 ± 0.04	0.094
Al_09b	Plasma condensation; uncoated; nominal size: 0.04 μm	56.4 ± 0.16	0.039

[a]EEW, or electrical explosion of wires.
[b]Nominal, or declared by manufacturer.
[c]Below, sensitivity threshold.

products (CCP) [11–13] consist of two fractions: smoke-oxide particles (SOP) and agglomerates. The SOP with a typical size around 1 μm, formed by condensation of the gas-phase reaction products and combustion of the nonagglomerating metal, account for the largest part of the produced oxide, typically 80%. Agglomerates, consisting of Al and Al_2O_3, are formed from the oxide skin surrounding the original Al particle and by condensed phase surface reactions during the particle combustion. Enlargement of the metal particle size originally contained in the propellant can occur via agglomeration of the molten metal and oxide with size of the order of 100 and even 1000 μm. Details of the sintering-agglomeration process affect [14,15] the site and extent of the overall combustion process as well as the size of the product oxide droplets. These properties (impacting burning rate, combustion efficiency, combustion stability, and slag formation) do in turn depend on the specific propellant formulation and operating conditions.

A. Ingredients Used

Ammonium perchlorate (AP) provided from two different suppliers was used: one called AP-1 from a propulsive supplier and another called AP-2 from a commercial supplier. Several Al powders (spheres or flakes), provided by international sources and covering both nanometric and micrometric size ranges, were employed; see Table 1 for a comprehensive summary. Mostly used in this paper are uncoated *n*Al particles of Russian production and low-cost commercial μAl flakes (with 50 μm characteristic size). The binder is based on hydroxyl-terminated polybutadiene (HTPB), a polyfunctional oligomer of butadiene which comes with hydroxyl groups. The binder also contains di-octil adipate (DOA) acting as a plasticizer, isophorone di-isocyanate (IPDI) acting as a curing agent, and a tin-based catalyst. Both HTPB R-20 (density 0.913 g/cm^3) and HTPB R-45 (density 0.985 g/cm^3) were used. With respect to the space-grade HTPB R-45, the R-20 version features a lower molecular mass and a lower viscosity that contributes to ease the mixing of compounds containing ultrafine powders. In all laboratory propellants bonding agents were not used.

B. Formulations Tested

A reference laboratory formulation consisting of 68% AP oxidizer, 17% HTPB binder, and 15% Al fuel was selected to investigate peculiar effects connected with *n*Al, emphasizing in particular differences with respect to the usual μAl. In addition, several laboratory propellants all containing 83% mass fraction of solids, but different size distributions for both AP and Al were manufactured. Monomodal AP range is 75 ± 5 μm. For practical reasons of supply, only bimodal AP fractions consisting of a blend of coarse (150 ± 10 μm) and fine (75 ± 5 μm) particles could be used; unfortunately, this configuration is known to be less than ideal since overlapping of AP powders is likely to occur. Bimodal Al size distributions are based on a mixture of coarse fraction (30 or 50 μm) and nanometric powder (0.1 to 0.2 μm). The coarse to fine (c/f) ratio was variable for Al mixtures, but always kept as 4-to-1 for AP mixtures.

Out of the many AP/HTPB/Al compositions tested, two laboratory propellant series and an industrial one are discussed in this paper (Tables 2–4). Series I traces the effects of a partial replacement of μAl type 06 with *n*Al type 02b (see Table 2) moving through five Al compositions. The Al content changes gradually from 100% μAl flakes (P_06) to 100% *n*Al particles (P_02b). The remaining three propellants (P_07b, P_08, P_09) feature a bimodal Al distribution, with 50 or 30 μm (coarse) and 0.17 μm (ultrafine) particle sizes, according to the indicated c/f ratio.

Series II is meant to assess how steady burning rate changes with Al particle size and thus includes only monomodal Al distribution

Table 2 First series of propellant formulations: bimodal AP-2, monomodal or bimodal Al, HTPB R-20 binder

Propellant short notation	AP supplier and granulometry, μm	Al (15%)		Binder (17%)
		Type	Nominal size	
P_06	AP-2; 70–80, 140–160	100% type 06	50 μm	HTPB R-20
P_07b	AP-2; 70–80, 140–160	80% type 06	50 μm	HTPB R-20
		20% type 02b	0.15 μm	
P_08	AP-2; 70–80, 140–160	50% type 06	50 μm	HTPB R-20
		50% type 02b	0.15 μm	
P_09	AP-2; 70–80, 140–160	50% type 05a	30 μm	HTPB R-20
		50% type 02b	0.15 μm	
P_02b	AP-2; 70–80, 140–160	100% type 02b	0.15 μm	HTPB R-20

Table 3 Second series of propellant formulations: bimodal AP-2, monomodal Al, HTPB R-20 binder

Propellant short notation	AP supplier and granulometry, μm	Al (15%)		Binder (17%)
		Type	Nominal size	
P_06	AP-2; 70–80, 140–160	100% type 06	50 μm	HTPB R-20
P_05	AP-2; 70–80, 140–160	100% type 05a	30 μm	HTPB R-20
P_03d	AP-2; 70–80, 140–160	100% type 03d	2.5 μm	HTPB R-20
P_04a	AP-2; 70–80, 140–160	100% type 04a	0.2 μm	HTPB R-20
P_01a	AP-2; 70–80, 140–160	100% type 01a	0.15 μm	HTPB R-20

Table 4 Third series of propellant formulations: bimodal or trimodal AP-1, monomodal Al, HTPB R-45 binder, with compositions given in volume percents

Propellant short notation	HTPB + Al + Fine AP (binder matrix or microstructure), %	Coarse AP %	Microstructure characteristic length, μm (see Sec. VI)
A	47.7	52.3	146
B	45.1	54.9	283
C	48.3	51.7	183
D	49.3	50.7	149

(see Table 3). Propellant P_05 includes 100% of space-grade spherical μAl type 05a (30 μm diameter). Propellant P_03d includes Al particles of 2.5 μm nominal size; propellant P_04a includes Al particles of 0.2 μm nominal size and protected by a hydrocarbon coating; propellant P_01a includes Al particles of 0.15 μm nominal size (nanosize aluminum obtained by electrical explosion of wires, or Alex®).

To allow a meaningful comparison of both effects, a common baseline propellant (called P_06) has been enforced for both series I and II. P_06 include 100% of μAl flakes type 06.

Series III is meant to study the agglomeration details for a variety of industrial μAl propellants, always of the type AP/HTPB/Al (Table 4). Experimental and theoretical tests were conducted with four formulations (denoted of as A, B, C, and D) using AP-1 as oxidizer and HTPB R-45 as binder. AP was a blend of coarse, medium, and fine (<10 μm) particles.

C. Propellant Surface Microstructure Texture

Filling of the propellant microstructure (i.e., the fine material distributed among the coarse oxidizer particles) is visualized with two different techniques in Fig. 1. Contrast the *n*Al surface texture, see Fig. 1 upper part, with that of μAl, see Fig. 1 lower part; each picture includes in its upper strip a mark for the 200 μm scale. The microstructure material includes binder, Al particles, and also the smallest AP particles making the oxidizer mass fraction. In both cases, the coarse oxidizer grains (bimodal AP-2) of irregular shape are well visible under ordinary light illumination. Energy dispersive x-ray analysis (EDX) illumination was used to reveal the Al distribution, showing a uniform and well-distributed scattering of *n*Al among the coarse AP particles.

III. Steady Burning Rate Measurements

A. Experimental Technique

Propellant samples ($4.5 \times 4.5 \times 30$ mm) of the tested formulations were burned in a nitrogen-flushed window bomb in order to

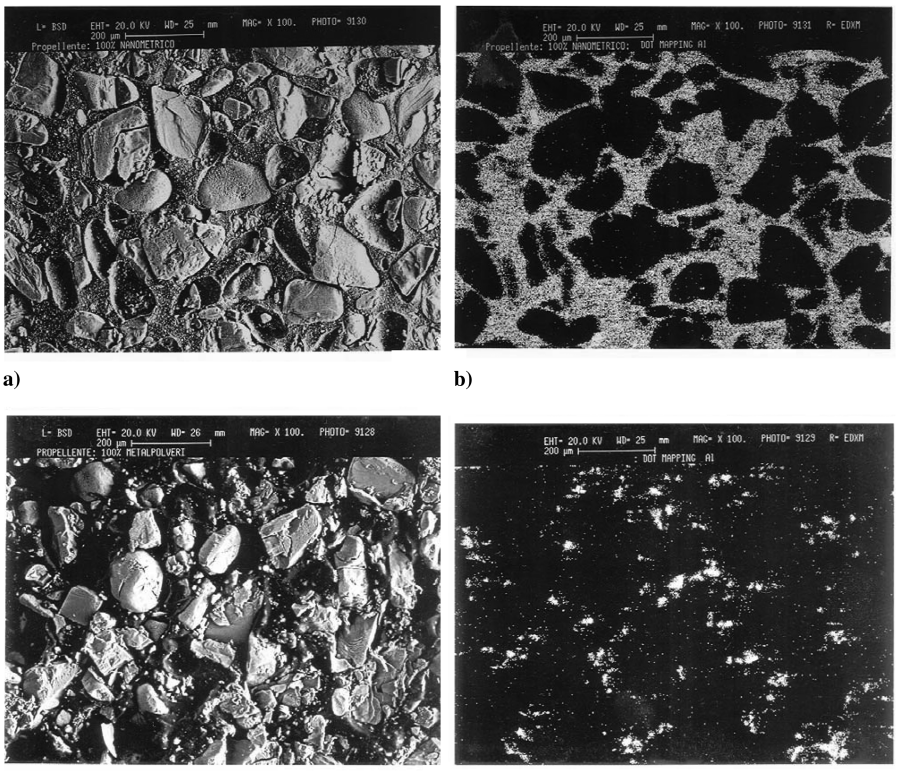

Fig. 1 Visualization of the propellant surface microstructure: parts a and b) *n*Al type 01a; parts c and d) μAl type 06. SEM images left, EDX images right (series I propellants, bimodal AP-2).

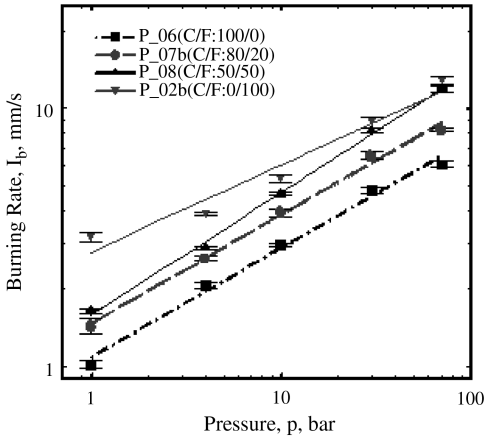

Fig. 2 Increasing steady burning rates with decreasing c/f fraction of Al powder; P_09 and P_05 (not shown), respectively, overlap P_08 and P_06 (series I propellants, bimodal AP-2).

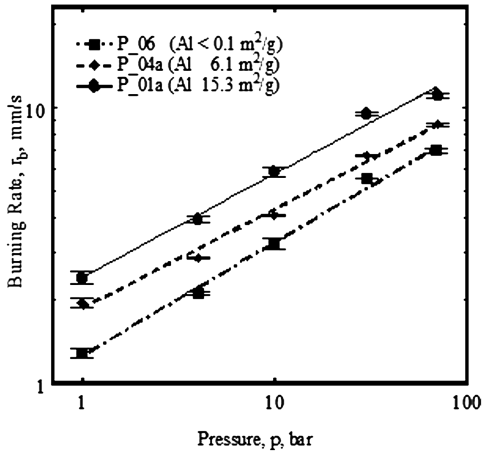

Fig. 3 Increasing steady burning rates for decreasing Al powder size; P_05 with 0.1 m^2/g Al and P_03d with 0.7 m^2/g Al (not shown) essentially overlap P_06 (series II propellants, bimodal AP-2).

measure the steady burning rate. Samples were ignited by a hot nichrome wire. Pressure was kept constant during the whole combustion process with a feedback pressure control system. Steady burning rates were measured in the range 1–70 bar, using an automated image processing technique from high-speed video recordings. At least three samples were used for each experimental point and for each sample several burning rate readings were performed, according to well-established Space Propulsion and Nanoenergetics Laboratory procedures [9,10].

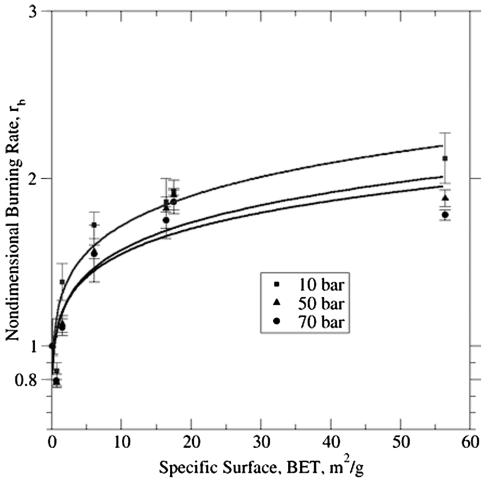

Fig. 4 Normalized steady burning rate vs BET specific surface, for propellants loaded with monomodal Al powders (see full list in Table 1), showing different sensitivity over the explored BET range.

B. Micrometric vs Nanometric Al Powder: Partial or Full Replacement

As shown in Fig. 2 propellant P_06, designated as baseline, has the lowest burning rate. All remaining formulations containing *n*Al exhibit significantly higher burning rates. By replacing 50 μm Al flakes with the same amount of 0.1 μm *n*Al (type 01a), burning rate approximately increases by 40% (P_07b), 60% (P_08), and 100% (P_02b), respectively, corresponding to 20, 50, and 100% nanometric replacement of the μAl powder. Thus, steady burning rates increase by increasing the fraction of *n*Al. For both monomodal Al distribution propellant (P_05) and bimodal Al distribution propellant (P-09), no significant burning rate difference is observed by replacing 50 μm Al flakes with 30 μm Al spheres (compare propellant P_05 to P_06 and propellant P_09 to P_08).

C. Micrometric vs Nanometric Al Powder: Parametric Size Effect

The second propellant series shows a similar trend, as illustrated in Fig. 3. Formulations including different *n*Al powders (type 04a and 01a, propellants P_04a and P_01a, see Table 3) feature significantly higher burning rates, while Al particles in the range 2.5 to 50 μm make no appreciable difference.

D. Micrometric vs Nanometric Al Powder: Specific Surface Effect

A systematic survey of steady burning rate using further Al powders and either AP yielded the general trend illustrated in Fig. 4; additional specific effects were reported previously [7–10]. In general, under the explored operating conditions, steady burning rates measured for propellants loaded with a variety of Al powders show different sensitivity over the explored Brunauer–Emmett–Teller (BET) range of Al and yield an appreciable increase only for BET above, say 2 m^2/g.

E. Summary of Steady Burning Rate Measurements

The Vieille ballistic laws and densities measured for the indicated laboratory compositions are summarized in Table 5. Monomodal *n*Al formulations (P_01a and P_04a, for example) yield appreciably higher propellant densities than μAl formulations (P_05 and P_06).

In series I propellants, replacing μAl with *n*Al, bimodal Al compositions feature (with respect to the baselines P_05 and P_06 and with growing fraction of *n*Al replacement) a significant increase of burning rates while pressure sensitivity is slightly increased (manual mixing).

In series II propellants, decreasing *n*Al size, monomodal Al compositions feature (with respect to the baselines P_05 and P_06) a prominent increase of burning rates in the range 0.1–0.2 μm (P_04a, P_01a) while pressure sensitivity is only slightly affected.

Table 5 Best fitting of Vieille steady burning rate law for several tested propellants

Propellant short notation	Density g/cm^3	Experimental/ theoretical density	Vieille burning rate law, $r_b = ap^n$	
			a, mm/s	n
P_01a	1.67	0.98	2.42 ± 0.07	0.38 ± 0.01
P_02b	1.65	0.97	2.00 ± 0.04	0.44 ± 0.01
P_03d	1.56	0.91	1.46 ± 0.06	0.37 ± 0.01
P_04a	1.70	0.99	1.86 ± 0.04	0.36 ± 0.01
P_05	1.52	0.89	1.32 ± 0.03	0.39 ± 0.01
P_06	1.59	0.93	1.26 ± 0.03	0.41 ± 0.01
P_07b	1.60	0.94	1.47 ± 0.03	0.42 ± 0.01
P_08	1.63	0.95	1.58 ± 0.03	0.48 ± 0.01
P_09	1.67	0.98	1.57 ± 0.07	0.47 ± 0.02

Under common operating conditions, the pressure sensitivity of steady burning rates is not significantly affected. This implies that the pressure dependence of the effective heat feedback determining the steady burning rate of the investigated propellants is essentially unchanged by the additional heat source due to metal (nAl) combustion. Thus, the role of diffusive and kinetic factors remains essentially the same. This circumstance can be related to the influence on steady burning rate of both the first and second stage of heterogeneous burning of metal [16].

IV. Ignition Delay

While ignition of solid propellants is a well-investigated subject, the behavior of compositions including ultrafine powders is scarcely investigated [17,18]. The ignition delay vs radiant flux, from a continuous wave CO_2 laser source, was measured for several of the propellants investigated in this research project. The baseline propellant (P_06) showed the highest ignition delay; the reason can be attributed also to the Al large thermal conductivity, which slows down the surface temperature rise. By progressively replacing μAl with nAl, while keeping constant the total Al mass fraction (15%), the ignition delay decreases. The importance of metal ignition temperature has recently been discussed in some detail [16]. During laser heating, the enhanced reactivity of nAl powders manifests as an earlier buildup of the transient flame (leading to self-sustained combustion regime) with respect to not only μAl, but even unmetallized compositions. This is in qualitative agreement with the reported possible lower melting temperature [19] of nAl and quicker ignition [20] of nAl-based reactive mixtures. Further results of metal powder reactivity in hot gaseous streams confirmed [21] this trend. Detailed results are not reported to save space.

V. Flame Structure, Burning Surface, and Microstructure of Metallized Propellants

A high-speed digital color video camera, up to 2,000 fps at full resolution, allowed a convenient visualization of combustion surface phenomena. Tests were performed in a horizontal combustion chamber with optical view ports up to 30 bar. Combustion occurred in a nitrogen atmosphere with the pressure regulated by an automatic control system. Recording was performed with a high spatial resolution video system with a long-range microscope; light was provided by a cold-light source. Care was taken to exclude burning transients from video recording. Calibration was repeated for each test session.

To distinguish the different ways that the complex phenomena of agglomeration overall manifest, the following nomenclature is enforced in this paper: the word agglomeration is reserved to the formation of the spherical drops of liquid metal and oxide in combustion, while the word aggregation is reserved to the formation of the partially oxidized flakes of irregular shape seen at or near the burning surface (an intermediate step between the initial metal load and the possible final agglomerates). Agglomerates always imply a loss of the initial particle individuality; aggregates are agglomeration precursors and may keep some reminiscence of the initial particle individuality. As defined, both agglomeration and aggregation are typically manifested by Al burning. In addition, it is convenient to reserve the word cohesion to "a portion of a substance cleaving together in a thick nondescript mass" (Webster's Dictionary).

A. Cold Cohesion vs Hot Aggregation/Agglomeration

Cold cohesion, a characteristic trait of the fluffy nanosized particles, takes place at room temperature (or close to) during storage, handling, and manufacture of the propellant. This kind of pulling together is responsible for microsized clusters reducing the specific surface of nanosized ingredients, and thus works against the major, although not unique, rationale of their enhanced reactivity. All precautions should be taken, including coating of the particles, to lessen the propensity of nAl to cold cohesion (i.e., clots or lumps of particles). Hot agglomeration is a well-known trait of μAl occurring under high temperatures at the burning surface or in the gas phase of the combustion wave.

B. Flame Structure of AP-Based Composite Propellants

For the explored operating conditions, the well-known [22,23] underlying unmetallized flame structure appears affected to a modest extent, as revealed by the minor changes of the burning rate pressure sensitivity. Al particle size affects burning according to the following trends:

1) Metal powders in the nanometric range show a remarkable steady burning rate increase with decreasing nAl size and point out a primary effect of specific surface increase, typically by at least 2 orders of magnitude from μAl to nAl.

2) For μAl propellants, the condensed combustion products result from a competition between the homogeneous diffusion flames in the gas phase yielding SOP and the heterogeneous reaction of liquid Al [24,25]. The fraction of the metal participating in aggregation/agglomeration processes depends on the propellant properties [26–28]. The first stage of metal burning by agglomeration is carried out within the skeleton layer whose features determine [29] burning properties. In either case (burning of metal with or without agglomeration), μAl particles feature a spacewise distributed burning overlapping the underlying unmetallized flame structure but extending much beyond the gas-phase flame thickness, and thus little affecting steady burning rates.

3) Qualitative and quantitative information was obtained comparing the growth mechanism of aggregation/agglomeration processes for propellants loaded with metals of different BET

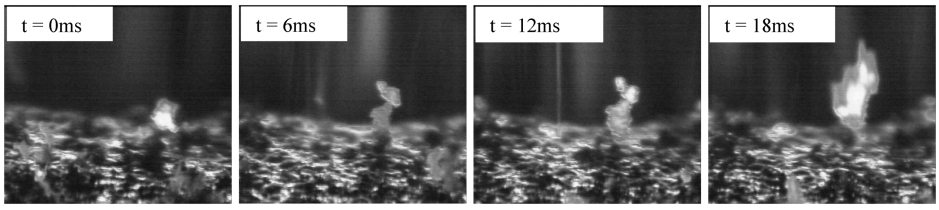

Fig. 5 Burning surface of 50 μm Al flakes propellant at 2 bar showing protruding clusters (filigrees) and aggregate inflammation just before agglomeration (P_06, exposure time 1/500 s).

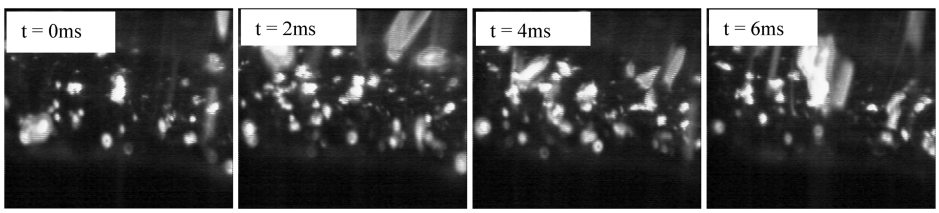

Fig. 6 Burning surface of a 0.15 μm nAl propellant tested at 2 bar (P_02b, exposure time 1/4000 s).

surfaces. Although following the same succession of events, the burning mechanism of *n*Al particles is plainly different, as discussed in the next sections.

C. Burning Surface of Metallized Propellants

Burning processes at or near the combustion surface were contrasted for μAl vs *n*Al propellants. Figures 5 and 6 show some frames taken from tests performed at 2 bar for propellants P_06 and P_02, containing 100%, respectively, of 50 μm and 0.15 μm Al particles. The brightness of the region immediately above the burning surface can be associated to the rapid combustion of *n*Al in that region, which enhances near-surface heat release, thus increasing burning rate. This remark is in qualitative agreement with the spectroscopic data by Weiser et al. [30] and explains the burning rate augmentation shown in Figs. 2 and 3. In agreement with Trubert et al. and ONERA [31], further basic differences and a possible explanation are discussed hereinafter.

D. Micrometric Al Powder: Agglomeration Controlled

Following the pioneering work by Price [24,25] during binder and oxidizer decomposition the metal particles, confined in the microstructure among the coarse AP grains, warm up and reach the burning surface. Aluminum particles are naturally covered by a porous and refractive Al_2O_3 coating (unless of intentional provisions). The two materials have different thermal expansion coefficients and melting temperatures ($T_{\mathrm{melt}_{Al2O3}} = 2345$ K vs $T_{\mathrm{melt}_{Al}} = 933$ K); in addition, solid and liquid Al have different density yielding after heating a volumetric expansion of about 6%. All of these effects help the formation of clots of irregular shape in the skeleton layer of the burning propellant surface [11–13]. In particular, clusters of elongated shape (filigrees [32]) are observed, accumulating on the burning surface, and protruding into the hotter regions of the gas phase, as typical of class B propellants (with the metal ignition temperature higher than the decomposition temperature of carbonaceous elements, yielding a skeleton layer made by the initial metal particles fastened among themselves). Then, a progressive but intense heating changes these protruding clots into reacting and hot aggregates, whose quick inflammation yields particle coalescence. The final result is a single drop in combustion with the characteristic round shape.

Under the proper thermal and oxidizing conditions, ignition of aggregates and transition to agglomerates occurs [24,25] when the protective oxide coating surrounding Al particles is cracked by fractures due to heating. Mainly the near-surface hot AP/binder flamelets, called leading-edge flames (LEF), are suspected to be responsible for this phenomenon. After formation, the burning agglomerate particle (chiefly a mixture of liquid Al and liquid Al_2O_3, with a solid lobe of Al_2O_3) keeps on growing until detachment. The whole sequence is clearly illustrated in Fig. 7, showing the transition process for an industrial propellant at 5 bar. A vivid example of the agglomeration results in the particle-laden flame zone for a typical highly loaded μAl propellant is shown in Fig. 8, taken for another industrial propellant at 5 bar. For such industrial propellants, the observed [33–35] average agglomerate size is slightly above 250 μm at 5 bar and shrinks by almost 50% at 25 bar; see discussion in Sec. VI. For μAl, most of the heat release occurs far from the burning surface.

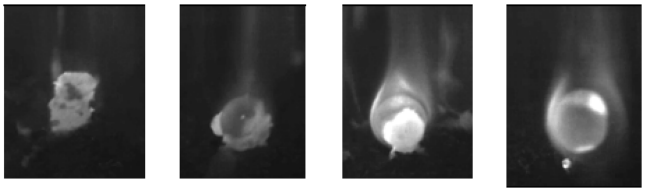

Fig. 7 Sequence capturing aggregate to agglomerate conversion for industrial propellant A tested at 5 bar, 2000 fps, nominal magnification 3 times.

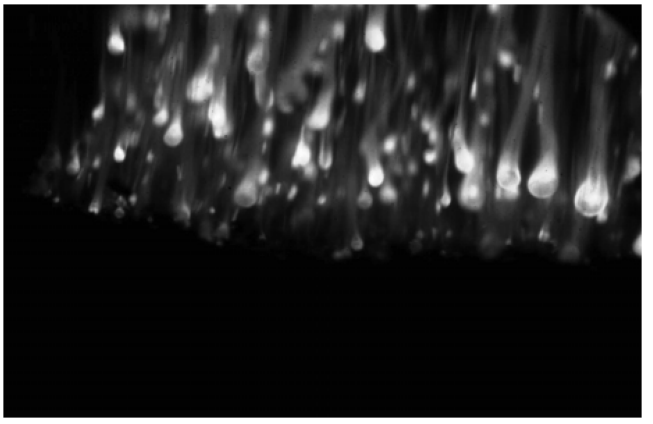

Fig. 8 Particle-laden flame zone due to Al combustion at some distance from the burning surface for industrial propellant D tested at 5 bar.

E. Nanometric Al Powder: Aggregation Controlled

Specific attention was devoted to the combustion surface phenomena, probably the controlling zone for heat release of *n*Al burning. The results of Fig. 9 show the details of the near burning surface region for P_01a propellant, revealing an unusual coral like formation, reminiscent of the propellant microstructure visualized in Fig. 1 (top pictures), exuding from the propellant microstructure. These pictures, validated for a variety of formulations and over a range of pressure, allow assigning the investigated propellants to class nano**B** propellants [16].

Aggregation/agglomeration phenomena, although following the same succession of events, bluntly differ for μAl and *n*Al particles. Chemical analyses of the friable exudation flakes reveal the presence of metal oxidation products together with some intermediate combustion products and possible residual unburned metal. Exudation is due to *n*Al aggregation probably starting in depth. Once the aggregation flakes have emerged at the burning surface, they can complete their oxidation/combustion while crumbling into CCP particles reminiscent of their original size (micrometric or submicrometric). Little agglomeration is observed following the exudation of aggregation flakes at the surface. No significant inflammation (transition of burning into gas-phase mode) takes place, but the burning surface appears much more luminous thanks to the very large number of *n*Al flakes completing their oxidation (burning in heterogeneous mode) at/near the burning surface. Although agglomeration is possible for *n*Al as well, size and combustion times [36–38] of *n*Al particles are so small that its consequences are measurably reduced; in addition, resealing after

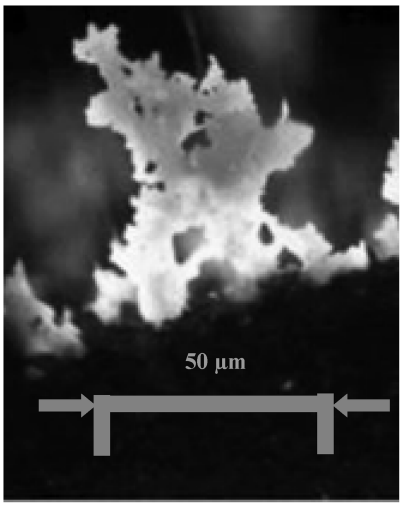

Fig. 9 Burning surface of a 0.15 μm *n*Al propellant tested at 10 bar (P_01a, exposure time 1/4000 s). The oxidized metal flakes look like a 3-D replica of the *n*Al distribution visualized in Fig. 1.

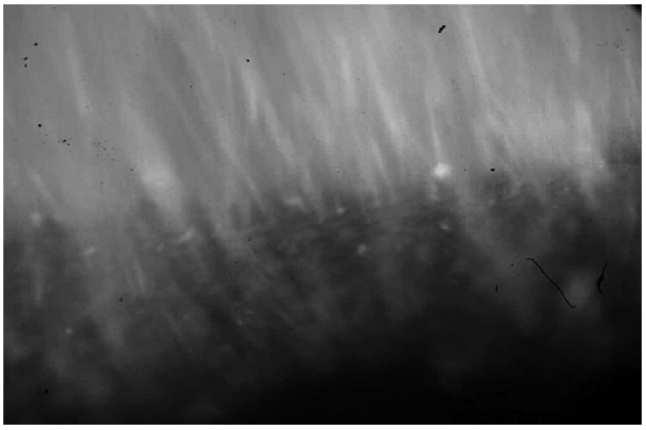

Fig. 10 AP/polypropylene glycol-based composite formulation containing *n*Al type 01a burning at 10 bar: fine aggregate emerging on surface by exudation and reduced transition to spherical agglomerates within short distance from the burning surface.

oxide layer crack is less likely to occur [15]. The kind of image seen in Fig. 8 for the particle-laden flame zone of μAl propellants is replaced by the blurred image of Fig. 10 for *n*Al propellants.

Aggregation, seen for μAl propellants only for short instants preceding agglomeration, is the main visible stage for *n*Al propellants. The distinctive feature of μAl in the studied formulations is agglomeration, while the distinctive feature of *n*Al burning is aggregation. With respect to μAl particles, *n*Al particles feature the combined effects of earlier ignition and quick premixed oxidation (possibly in depth), followed by oxidation completion at or very close to the burning surface. Thus, at the propellant surface layer, combustion of *n*Al particles is almost concluded, whereas μAl particles are just starting to react. This essentially heterogeneous burning mechanism yields smaller agglomerates of unusual structure, consisting of a central metal core surrounded by an oxide layer [16]. This in turn implies the absence of slag formation losses and also a probable increase of combustion inefficiency, as pointed out by results shown in Fig. 11. This figure contrasts, under ideal thermochemical conditions, the combustion temperature and products composition with the corresponding values achieved if only a fraction of the available fine AP reacts in the propellant microstructure, yielding a relatively low-temperature (due to the very fuel-rich mixture ratio of the local premixed flame) but prompt metal oxidation. Unless oxidation is fully completed downstream, combustion inefficiencies will arise. In exploratory tests with *n*Al type 01 burning under subatmospheric pressure, about 80% γ-Al_2O_3 and δ^*-Al_2O_3 were recovered, while up to 10% was unburned Al and the remaining CCP consisted of intermediate products, such as Al_2OC and Al_4C_3. Similar analyses were performed at ONERA [31].

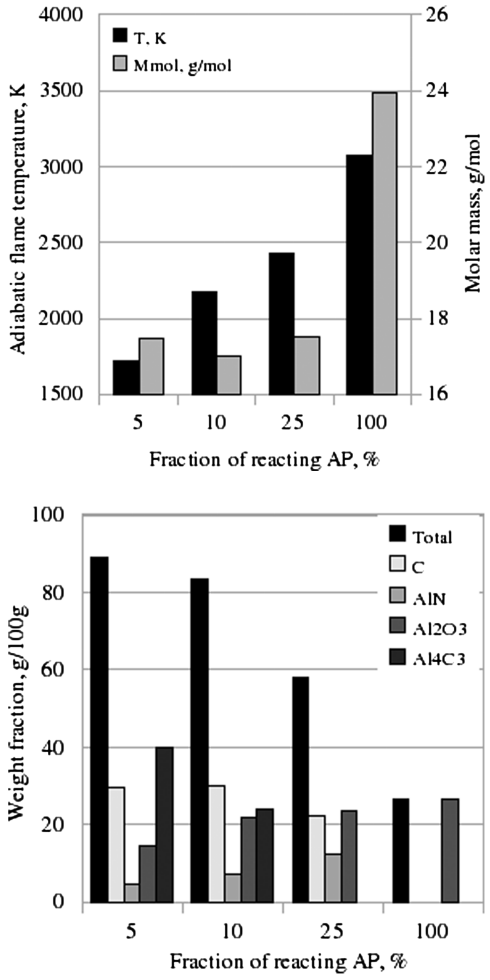

Fig. 11 Computed adiabatic temperature (top), molar mass (top), and main combustion products (bottom) for model propellant E, under ideal equilibrium conditions at 30 bar, for an increasing fraction of reacting AP. For 100% reacting AP, temperature is maximum and Al_2O_3 is the only CCP; for reduced fractions of AP, temperature is sensibly less and several intermediate CCP appear.

Although the variety and complexities of the observed phenomena require further studies, the enhanced reactivity of *n*Al is well manifest. The average size of CCP is sharply reduced, as confirmed in other studies [39,40], with obvious advantages in terms of nozzle expansion efficiency. But the resulting overall specific impulse efficiency will depend on the combination of all of the above factors.

Possible mechanisms responsible for the formation of the *n*Al flakes, for the considered class of propellants, include propellant manufacturing, propellant storage, and propellant heating during combustion (or a combination of all of them). The assumption that the contact between initial particles of *n*Al for propellants such as nano**B** is related to technology factors was already discussed [16]. At any rate, under any circumstances, the conductive thermal wave preceding the burning surface is able to warm up the ***n*Al** particles within the propellant microstructure to temperatures of the order of the ignition temperature, recalling the enhanced ***n*Al** reactivity (see Sec. IV). The intimate mixing with the surrounding decomposition products of the fine AP fractions and binder, favoring a local underoxidized premixed flame, promotes the formation of partially oxidized and intermediate metallized flakes (prompt metal oxidation). Depending on steady burning rate (i.e., pressure), type of binder, fine oxidizer size, and fraction, some unburned metal will also contribute to the flake formation.

F. Mitigation of Cold Cohesion and Hot Aggregation/Agglomeration

Coating Al particles with high-melting metal films (e.g., Ni, Cu, Fe) decreases hot agglomeration [41] by making μAl ignition easier probably thanks to highly exothermic intermetallic reactions at Al melting; a similar effect can also be reached by coating with organic substances [42]. Coatings can also be used to mitigate the propensity to cold cohesion.

VI. Agglomerate Size Prediction

Agglomeration of metal powders significantly affects delivered specific impulse, due to combustion inefficiencies and two-phase flow losses. Depending on the specific set of ingredients and operating conditions, complex phenomena of aggregation/agglomeration may begin below the burning surface, continue at the propellant burning surface, and extend even to very large distances in the gas-phase. A variety of peculiar phenomena may take place during the agglomerate lifetime, including SOP deposition on the agglomerate, changes in the agglomerate structure due to metal burning with the corresponding oxide lobe growth, and rotating-translating motion through the surrounding gaseous atmosphere. Depending on the details, metal agglomerates may be of matrix type, or cap oxide, or hollow bag, or metal core covered by an oxide layer [28,43].

The objective of the theoretical part of this work is to understand how the details of the propellant composition affect the agglomerate average size at their very birth, and thus be able to predict this value. The correlation with the propellant microstructure was systematically investigated for a range of multimodal propellant formulations of current industrial production. The percent volumetric composition of the four tested metallized solid propellants is reported in Table 4. Note that, for the purposes of the statistical analysis carried out, metal and fine AP powders can be disregarded as separate ingredients and be rather considered as part of the HTPB binder matrix (the propellant microstructure). The proposed analysis, based on statistical geometry considerations [44–46], is currently restricted to μAl propellants.

To be able to predict the agglomerate average size at their birth, a statistical analysis is performed of the spatial distribution of the oxidizer particles in the bulk matrix of the tested aluminized composite solid propellants. Microstructures of random composites are usually studied by means of micrographs or topographic data, at high levels of magnification. Recently a new approach, cheaper and easier, has involved numerical analysis of statistically equivalent computer-generated microstructures of propellant sections. A new algorithm was developed that does not make use of cuts of original 3-D packings to originate the sections, but it directly creates 2-D sections. This approach has been compared with sections stemming from certified 3-D for evaluation and has proved to satisfactorily reproduce the trend of 3-D derived sections curves. For the numerical algorithm of two-points probability calculation, the standard procedure proposed by Rintoul and Torquato [47] and Smith and Torquato [48] in 1988 has effectively been implemented [45].

In the field of solid propellants, simulation of realistic heterogeneous material sections is done by a packing algorithm, whose inputs are the relevant pieces of information about propellant composition and ingredient distributions. A first simple packing algorithm can be a random positioning of particles inside a surface or a volume, followed by successive phases of refinement in order to avoid overlapping of particles. Recent techniques resort to a dynamic approach, where a momentum equation is written for each particle, under the effect of reciprocal repulsion or attractive functions [49]. Another modern technique of rigid sphere packing uses an event-driven molecular dynamics approach [50]. In this approach, particles are advanced between events, where an event is loosely defined as anything that changes a particle's state. The event could be a binary collision, a collision between a particle and a domain boundary, or a transfer of a particle across an internal or external boundary. Instead of advancing the particles by a fixed time step, particles are advanced to the next event time [44].

Evaluating the two-points probability functions (oxidizer–oxidizer, binder–binder, and the phase change curves) allows defining a characteristic size and a characteristic time in the condensed phase of the energetic material microstructure. The characteristic size is defined by the distance giving the maximum probability, moving from an AP particle or a binder zone, to see a transition, respectively, to binder or AP, while the characteristic time is just the characteristic size/steady burning rate. An intuitive geometrical interpretation of the characteristic size is that it is equal to half of the average distance between coarse oxidizer particle boundaries, i.e., it determines the size of a pocket.

Experimental results point out that such a characteristic time correlates the average size of the Al agglomerates generated at or near the burning surface. The final result [45] is a linear dependence of the agglomerate average size on the characteristic time of the heterogeneous energetic material microstructure. With reference to Table 4, the microstructure characteristic size is the parameter that separates the μAl propellants under test. The large value exhibited by industrial propellant B indicates that much more space is available in this case between large oxidizer grains for metal aggregation with respect to other propellants. In turn, this condition favors the creation of large agglomerate sizes.

Table 6 Measured average diameter and standard deviation of agglomerates

Pressure bar	Average diameter, D_{43agg}, μm, and standard deviation			
	A	B	C	D
5	264 ± 14.6	NAv	344 ± 13.6	276 ± 7.8
10	266 ± 11.5	NAv	251 ± 5.4	181 ± 6.3
20	167 ± 5.7	454 ± 31.2	210 ± 14.5	148 ± 3.9
25	142 ± 4.0	362 ± 11.5	184 ± 6.5	145 ± 4.8

A close comparison with the experimental results collected from a variety of microaluminized AP/HTPB-based propellants show a good agreement of the expected values of the incipient agglomerates with the experimental ones, for combustion pressures up to 25 bar (the maximum value that the available optical setup could explore). The average agglomerate diameters vs pressure are reported in Table 6; the statistical uncertainty of the measurements is also indicated. The results obtained confirm for the investigated propellants the essential influence of their structure on the agglomerate size.

VII. Conclusions

AP/HTPB-based aluminized composite solid rocket propellants, containing *n*Al particles, show faster steady burning rates compared with the corresponding propellants containing μAl particles. This increase is mainly determined by the intense energy released by *n*Al particle oxidation completion very close to/above the burning surface following a kind of prompt partial oxidation at/below the burning surface. Nanosize Al particles manifest a strong reactivity mainly due to their increased specific surface (see Table 1) notwithstanding the simultaneous decrease of active Al content (typically, from 99.6% of 17 μm Al to 88.2% for Alex®). The number and speed of particles/agglomerates gradually increase with decreasing μAl size in the range $90 - 15$ μm, while a remarkable decrease of flame heterogeneity is observed for *n*Al in the range 0.1–0.2 μm. Steady burning rates are not affected by particles in the micrometric range (say, BET ≤ 2 m^2/g) but strongly increased by decreasing size particles over the explored nanometric range; for very small particles, the appreciable decrease of active metal hinders a further increase of steady burning rate. Pressure exponents showed only minor changes within the limits of the experiments (see Table 5).

Also for ignition, an appreciable decrease was found for *n*Al particles in the range 0.1–0.2 μm, while little effect was observed for μAl.

The importance of the two different effects of metal agglomeration for μAl and metal aggregation (prompt metal oxidation) for *n*Al was shown. Smaller CCP sizes imply reduced specific impulse losses, and also reduced particulate damping especially at low pressures. However, the exact results depend on the many details of the propellant formulation: in particular, the pressure exponent of steady burning rates has been observed to follow different trends according to the specifics of the composition and operating conditions. This fact suggests that, in addition to the sheer increase of the specific surface, other subtle chemical and physical factors (intermetallic compounds, crystalline structure, etc.) may be important in *n*Al enhanced reactivity. Furthermore, it is necessary to take into account that the way of inserting *n*Al in the propellant influences cold cohesion of particles.

In summary, clear support has been collected for improved ballistic properties and reduced hot agglomeration using *n*Al. But while density and specific impulse are improved, cost and safety somewhat aggravate. Cold cohesion (typical of *n*Al) and hot agglomeration (typical of Al in general) phenomena control the actual size of the metal particle before and during combustion. This in turn impacts many aspects of propulsive systems.

A systematic analysis is currently underway to elucidate the propellant microstructure role in controlling the aggregation to agglomeration transition for a variety of metal fuels. Based on the details of the propellant microstructure, one can predict [45] the incipient (at the burning surface) agglomerate size of microaluminized propellants. But the propellant structure description, no matter how accurate, is not enough to evaluate agglomerate size under all

circumstances. Full understanding of the aggregation vs agglomeration effects opens the path [51,52] to improved ballistic performance by mitigating two-phase flow losses.

Most of the *n*Al particles used in this research program had only a natural coating of oxide layer to protect against inadvertent ignition and slow down aging; however, the natural passivation of oxide layer decreases performance. The next studies will focus on coated *n*Al particles for a range of goals: passivation against natural oxidation and aging, cutback of cold cohesion propensity, reduction of hot agglomeration phenomena, and increase of powder energy contents. However, an intentional passivation coating [53] meant to prolong storage lifetime not only decreases active Al (from 88.2% of Alex® to 86.1% of L-Alex®) but was also shown to favor cold cohesion.

Acknowledgments

Financial support by Avio Space Propulsion, Colleferro, Italy (Contract C98044) for μAl investigations is gratefully acknowledged. The authors would like to acknowledge the fond memory of B. N. Kondrikov, who first suggested the importance of indepth chemical reactions and participated in the initial phases of this investigation. Special thanks are due to Woodward Waesche and Hugh McSpadden for useful discussions.

References

[1] Gen, M. Ya., Frolov, Yu. V., and Storozhev, V. B., On Combustion of Particles of Subdispersed Aluminum, *Combustion, Explosion and Shock Waves*, Vol. 14, No. 5, 1978, pp. 153–155.

[2] Gen, M. Ya., Ziskin, M. S., and Petrov, Yu. I., *Proceedings of the USSR Academy of Sciences*, Vol. 127, 1959, p. 366.

[3] Ivanov, G. V., and Tepper, F., "Activated Aluminum as Stored Energy Source for Propellants," *Challenges in Propellants and Combustion 100 Years after Nobel*, edited by K. K. Kuo, Begell House, New York, 1997, pp. 636–645.

[4] Barbee, T. W., Jr., "Multilayer Synthesis by Physical Vapor Deposition," in *Synthetic Modulated Structures*, edited by L. Chang, and B. C. Giessen, Academic Press, New York, 1985, pp. 313–337.

[5] Babuk, V. A., and Salimullin, R. M., "Nanoparticles as Component of High-Energy Condensed Systems," *Proceedings of the Sixth All-Russia Conference Intrachamber Processes and Burning in Installations on Solid Propellants and in Artillery Systems*, Institute of Applied Mechanics of the Russian Academy of Sciences, Izhevsk, Russia, Sept. 2008, pp. 292–301.

[6] Yetter, R. A., Risha, G. A., and Son, S. F., "Metal Particle Combustion and Nanotechnology," *Proceedings of the Combustion Institute*, Vol. 32, 2009, pp. 1819–1838. doi:10.1016/j.proci.2008.08.013

[7] Meda, L., Marra, G. L., Braglia, R., Abis, L., and Gallo, R., "A Wide Characterization of Aluminum Powders for Propellants," *Ninth International Workshop on Combustion and Propulsion*, edited by L. T. DeLuca, L. Galfetti, and R. A. Pesce-Rodriguez, Grafiche GSS, Bergamo, Italy, 2004.

[8] Galfetti, L., Severini, F., DeLuca, L. T., Marra, G. L., and Meda, L., "Ballistics and Condensed Combustion Residues of Aluminized Solid Rocket Propellants," *Ninth International Workshop on Combustion and Propulsion*, edited by L. T. DeLuca, L. Galfetti, and R. A. Pesce-Rodriguez, Grafiche GSS, Bergamo, Italy, 2004, paper 18.

[9] Galfetti, L., Severini, F., DeLuca, L. T., and Meda, L., "Nano Propellants for Space Propulsion," *4th International Spacecraft Propulsion Conference*, European Space Agency, Sardinia, Italy, June 04. CD Proceedings SP-555/556/557, ISBN 92-9092-866-2/-867-0/-868-9.

[10] DeLuca, L. T., Galfetti, L., Severini, F., Meda, L., Marra, G., Vorozhtsov, A. B., Sedoi, V. B., and Babuk, V. A., "Burning of *n*Al Composite Rocket Propellants," *Combustion, Explosion and Shock Waves*, Vol. 41, No. 6, 2005, pp. 680–692. doi:10.1007/s10573-005-0080-5

[11] Babuk, V. A., Vassiliev, V. A., and Malakhov, M. S., "Condensed Combustion Products at the Burning Surface of Aluminized Solid Propellant," *Journal of Propulsion and Power*, Vol. 15, No. 6, 1999, pp. 783–793. doi:10.2514/2.5497

[12] Babuk, V. A., Vassiliev, V. A., and Sviridov, V. V., "Formation of Condensed Combustion Products at the Burning Surface of Solid Rocket Propellant," *Solid Propellant Chemistry, Combustion, and Motor Interior Ballistics*, edited by V. Yang, T. B. Brill, and W. Z. Ren, Vol. 185, AIAA Progress in Astronautics and Aeronautics, AIAA, Reston, VA, 2000, pp. 749–776.

[13] Babuk, V. A., Vassiliev, V. A., and Sviridov, V. V., "Propellant Formulation Factors and Metal Agglomeration in Combustion of Aluminized Solid Rocket Propellant," *Combustion Science and Technology*, Vol. 163, 2001, pp. 261–289. doi:10.1080/00102200108952159

[14] Dokhan, A., Seitzman, J. M., Price, E. W., and Sigman, R. K., "The Effects of Al Particle Size on the Burning Rate and Residual Oxide in Aluminized Propellants," *37th AIAA/ASME/SAE/ASEE Joint Propulsion Conference and Exhibit*, AIAA Paper 2001-3581, Salt Lake City, UT, 08–11 Jul 2001.

[15] Dokhan, A., Price, E. W., Sigman, R. K., and Seitzman, J. M., "Combustion Mechanism of Bimodal and Ultra-Fine Aluminum in AP Solid Propellant," *38th AIAA/ASME/SAE/ASEE Joint Propulsion Conference and Exhibit*, AIAA Paper 2002-4173, July 2002.

[16] Babuk, V. A., Dolotkazin, I., Gamsov, A., Glebov, A., DeLuca, L. T., and Galfetti, L., "Nanoaluminum as a Solid Propellant Fuel," *Journal of Propulsion and Power*, Vol. 25, No. 2, 2009, pp. 482–489. doi:10.2514/1.36841

[17] Hermance, C. E., "Solid-Propellant Ignition Theories and Experiments," in *"Fundamentals of Solid Propellants Combustion"*, edited by K. K. Kuo, and M. Summerfield, Vol. 90, AIAA Progress in Aeronautics and Astronautics, 1984, Chap. 5.

[18] Lengellé, G., Bizot, A., Duterque, J., and Amiot, J., "Allumage des Propergols Solides," *La Recherche Aérospatiale*, 1991, pp. 1–20.

[19] Tepper, F., and Kaledin, L. A., "Combustion Characteristics of Kerosene Containing Alex Nano-Aluminum," *Combustion of Energetic Materials*, edited by K. K. Kuo, and L. T. DeLuca, Begell House, New York, 2002, pp. 195–206.

[20] Vorozhtsov, A. B., Arkhipov, V., Bondarchuk, S., Korotkikh, A., and Kuznetsov, V., "Ignition and Combustion of Solid and Gelled Propellants Containing Ultra-Fine Aluminum," *Tenth International Workshop on Combustion and Propulsion*, edited by L. T. DeLuca, Grafiche GSS, Bergamo, Italy, 2003.

[21] Meda, L., Marra, G., Galfetti, L., Severini, F., and DeLuca, L. T., "Nano-Aluminum as Energetic Material for Rocket Propellants," *Materials Science and Engineering*, Vol. C 27, 2007, pp. 1393–1396.

[22] Guirao, C., and Williams, F. A., "A Model for Ammonium Perchlorate Deflagration Between 20 and 100 atm," *AIAA Journal*, Vol. 9, No. 7, July 1971, pp. 1345–1356. doi:10.2514/3.6355

[23] Babuk, V. A., Gamzov, A. V., Glebov, A. A., Dolotkazin, I. N., and Dosychev, A. V., "Structure of Composite Metallized Solid Propellants and its Role during Burning," *Khimicheskaya Fizika i Mesoskopiya*, Vol. 8, No. 1, 2006, pp. 33–45 (in Russian).

[24] Price, E. W., "Combustion of Aluminum in Solid Propellant Flames," *AGARD PEP 53rd Meeting on Solid Rocket Motor Technology*, Paper 14, AGARD, Paris, France, 1979.

[25] Price, E. W., "Combustion of Metallized Propellants," *Fundamentals of Solid Propellants Combustion*, edited by K. K. Kuo, and M. Summerfield, Vol. 90, AIAA Progress in Aeronautics and Astronautics, AIAA, New York, 1984, Chap. 9.

[26] Babuk, V. A., Glebov, A. A., and Dolotkazin, I. N., "Burning Mechanism of Aluminized Solid Rocket Propellants Based on Energetic Binders," *Propellants, Explosives and Pyrotechnics*, Vol. 30, No. 4, 2005, pp. 281–290. doi:10.1002/prep.200500012

[27] Babuk, V. A., Vasilyev, V. A., Glebov, A. A., Dolotkazin, I. N., Galeotta, M., and DeLuca, L. T., "Combustion Mechanisms of AN-Based Aluminized Solid Rocket Propellants," *Ninth International Workshop on Combustion and Propulsion*, edited by L. T. DeLuca, L. Galfetti, and R. A. Pesce-Rodriguez, Grafiche GSS, Bergamo, Italy, 2004.

[28] Babuk, V. A., Glebov, A., Dolotkazin, I., Conti, A., Galfetti, L., DeLuca, L. T., and Vorozhtsov, A., "Condensed Combustion Products from Burning of Nanoaluminum-Based Propellants: Properties and Formation Mechanism," *Advances in Aerospace Sciences*, Torus Press, Moscow, 2009, pp. 3–16.

[29] Babuk, V. A., "Properties of a Surface Layer and Regularities of Burning Metallized Solid Propellants," *Combustion, Explosion, and Shock Waves*, Vol. 45, No. 4, pp. 486–494, 2009.

[30] Weiser, V., Eckl, W., Eisenreich, N., Kelzenberg, S., Plitzko, Y., Poller, S., and Roth, E., "Burning Behavior of Aluminized Composite Propellants Including Nanoparticles," *Ninth International Workshop on Combustion and Propulsion* , edited by L. T. DeLuca, L. Galfetti, and R. A. Pesce-Rodriguez, Grafiche GSS, Bergamo, Italy, 2004.

[31] Trubert, J. F., Hommel, J., Lambert, D., Fabignon, Y., and Orlandi, O., "New HTPB/AP/Al Propellant Combustion Process in Presence of

Aluminum Nano-Particles," *Advancements in Energetic Materials and Chemical Propulsion*, edited by K. K. Kuo and K. Hori, Begell House, New York, 2008, pp. 98–121.

[32] Price, E. W., Sambamurthi, J. K., Sigman, R. K., and Panyam, R. R., "Combustion of Ammonium Perchlorate: Polymer Sandwiches," *Combustion and Flame*, Vol. 63, No. 3, 1986, pp. 381–413. doi:10.1016/0010-2180(86)90007-6

[33] DeLuca, L. T., "Burning of Aluminized Solid Rocket Propellants: from Micrometric to Nanometric Fuel Size," In *Theory and Practice of Energetic Materials*, edited by H. Ping, W. Yajun, and L. Shengcai, Vol. 7, Science Press, Beijing, China, 2007, pp. 277–289.

[34] DeLuca, L. T., and Galfetti, L., "Burning of Metallized Composite Solid Rocket Propellants: from Micrometric to Nanometric Aluminum Size," *Proceedings of the 3rd Asian Joint Conference on Propulsion and Power*, The Korean Society of Propulsion Engineers, Gyeongju, Korea, March 2008.

[35] DeLuca, L. T., Galfetti, L., Maggi, F., Colombo, G., Bandera, A., Cerri, S., and Donegà, P., "Burning of Metallized Composite Solid Rocket Propellants: Toward Nanometric Fuel Size," *Proceedings of ESA Space Propulsion 2008*, ESA, Crete, Greece, May 2008.

[36] Belyaev, A. F., Korotkov, A. I., and Frolov, Yu. V., "Ignition and Combustion of Single Particle of Small-Grained Aluminum," *Combustion, Explosion and Shock Waves*, Vol. 4, No. 3, 1968, pp. 323–330.

[37] Olsen, S. E., and Beckstead, M. W., "Burn Time Measurements of Single Aluminum Particles in Steam and Carbon Dioxide," *Journal of Propulsion and Power*, Vol. 12, No. 4, 1996, pp. 662–671. doi:10.2514/3.24087

[38] Widener, J. F., and Beckstead, M. W., "Aluminum Combustion Modeling in Solid Propellant Combustion Products," AIAA Paper 98-3824, 1998.

[39] Cerri, S., Galfetti, L., DeLuca, L. T., D'Andrea, B., and Cianfanelli, S., "Experimental Investigation of the Condensed Combustion Products of Micro Aluminized Solid Rocket Propellants," AIAA Paper 07-5766, July 07.

[40] K. Jayaraman, S. R. Chakravarthy, and R. Sarathi, "Behavior of Nano-Aluminum in Solid Propellant Combustion," AIAA Paper 08-5257, 2008.

[41] Shafirovich, E., Escot, P., Chauveau, C., Gökalp, I., Rosenband, V., and Gany, A., "Combustion of Single Aluminum Particles with Thin Nickel Coatings," *Novel Energetic Materials and Applications*, edited by L. T. DeLuca, L. Galfetti, and R. A. Pesce-Rodriguez, Grafiche GSS, Bergamo, Italy, 2004.

[42] Risha, G. A., Boyer, E., Wehrman, R. B., and Kuo, K. K., "Performance Comparison of HTPB-Based Solid Fuels Containing Nano-Size Energetic Powder in a Cylindrical Hybrid Rocket Motor," *38th AIAA/ASME/SAE/ASEE Joint Propulsion Conference and Exhibit*, AIAA Paper 2002-3576, July 2002.

[43] Babuk, V. A., Glebov, A., Arkhipov, V. A., Vorozhtsov, A. B., Klyakin, G. F., Severini, F., Galfetti, L., and DeLuca, L. T., "Dual-Oxidizer Solid Rocket Propellants for Low-Cost Access to Space," *In-Space Propulsion*, edited by L. T. DeLuca, R. L. Sackheim, B. A. Palaszewski, Grafiche GSS, Bergamo, Italy, Nov. 2005.

[44] Maggi, F., Stafford, S., Jackson, T. L., and Buckmaster, J., "Nature of Packs Used in Propellant Modeling," *Physical Review E: Statistical, Nonlinear, and Soft Matter Physics*, 77, No. 4, 2008, p. 046107. doi:10.1103/PhysRevE.77.046107

[45] Bandera, A., Maggi, F., and DeLuca, L. T., "Agglomeration of Aluminized Solid Rocket Propellants," *45th AIAA/ASME/SAE/ASEE Joint Propulsion Conference and Exhibit*, AIAA Paper 2009-5439, Aug. 2009.

[46] Maggi, F., Bandera, A., Galfetti, L., DeLuca, L. T., and Jackson, T. L., "Efficient Solid Rocket Propulsion for Access to Space," *Acta Astronautica*, Vol. 66, Nos. 11–12, pp. 1563–1573, 2009.

[47] Rintoul, M. D., and Torquato, S., "Reconstruction of the Structure of Dispersions," *Journal of Colloid and Interface Science*, Vol. 186, No. 2, 1997, pp. 467–476. doi:10.1006/jcis.1996.4675

[48] Smith, P., and Torquato, S., "Computer Simulation Results for the 2-Points Probability Function of Composite Media," *Journal of Computational Physics*, Vol. 76, No. 1, 1988, pp. 176–191.

[49] Rashkovskiy, S. A., "Structure of Heterogeneous Condensed Mixtures," *Combustion, Explosion and Shock Waves*, Vol. 35, No. 5, 1999, pp. 523–531. doi:10.1007/BF02674497

[50] Donev, A., Torquato, S., and Stillinger, F. H., "Neighbor List Collision-Driven Molecular Dynamics Simulation for Nonspherical Hard Particles: I. Algorithmic Details," *Journal of Computational Physics*, Vol. 202, No. 2, 2005, pp. 737–764. doi:10.1016/j.jcp.2004.08.014

[51] DeLuca, L. T., Marchesi, E., Spreafico, M., Bandera, A., Maggi, F., Colombo, G., Galfetti, L., Consaga, J. P., and Kosowski, B. M., "Agglomeration Effects in Metallized Solid Rocket Propellants," *Theory and Practice of Energetic Materials*, edited by L. I. Shengcai, W. Yajun, C. Fengxia, Z. Shanshan, and Z. Shuqiong, Vol. 8, Science Press, Beijing, 2009, pp. 258–270.

[52] DeLuca, L. T., Marchesi, E., Spreafico, M., Reina, A., Maggi, F., Rossettini, L., Bandera, A., Colombo, G., and Kosowski, B. M., "Aggregation vs Agglomeration in Metallized Solid Rocket Propellants," *Eighth International Symposium on Special Topics in Chemical Propulsion*, Begell House, New York, Nov. 2009.

[53] Cliff, M., Tepper, F., and Lisetsky, V., "Ageing Characteristics of Alex Nanosize Aluminum," *37th AIAA/ASME/SAE/ASEE Joint Propulsion Conference and Exhibit*, AIAA Paper 2001-3287, July 2001.

S. Son
Associate Editor